2PFC^{TM} (Two Pixels, Full Color): Image Sensor Demosaicing and Characterization

Daniel Tamburrino*

School of Computer and Communication Sciences

Ecole Polytechnique Fédérale de Lausanne (EPFL)

CH-1015 Lausanne, Switzerland

Jon M. Speigle, Douglas J. Tweet,† and Jong-Jan Lee

Sharp Laboratories of America

5750 NW Pacific Rim Blvd.,

Camas, WA, USA 98607-9489

Abstract

We propose a modification to the standard Bayer CFA and photodiode structure for CMOS image sensors, which we call 2PFC^{TM} (Two Pixels, Full Color). The blue and red filters of the Bayer pattern are replaced by a magenta filter. Under each magenta filter are two stacked, pinned photodiodes; the diode nearest the surface absorbs mostly blue light and the deeper diode absorbs mostly red light. The magenta filter absorbs green light, improving color separation between the blue and red diodes. We first present a frequency-based demosaicing method, which takes advantage of the new 2PFC^{TM} geometry. Due to the spatial arrangement of red, green, and blue pixels, luminance and chrominance are very well separated in the Fourier space, allowing for computationally inexpensive linear filtering. In comparison with state-of-the-art demosaicing methods for the Bayer CFA, we show that our sensor and demosaicing method outperform the others in terms of color aliasing, PSNR, and zipper effect. As demosaicing alone does not determine image quality, we also analyze the whole system performance in terms of resolution and noise.

*Electronic address: daniel.tamburrino@epfl.ch

†Electronic address: dtweet@sharplabs.com

I. INTRODUCTION

To improve color accuracy and spatial resolution, as well as reduce aliasing and demosaicing artifacts, a number of color filter array (CFA) patterns have been proposed as alternatives to the Bayer RGB pattern [1], a few of which are illustrated in Fig. 1. Stacked pixel structures, which make use of variation of the absorption depth with wavelength have also been proposed, both in silicon (Si) [2–12] and a-Si alloy [13] systems. Most notable among these is the Foveon triple junction CMOS image sensor [5–7], in which R, G, and B information is collected at each pixel without the need for color filters, thus eliminating the demosaicing algorithms and accompanying image artifacts. However, to achieve acceptable color separation, the total Si absorbing region has to be quite deep, requiring expensive epitaxial Si processes.

A particularly interesting structure was investigated by Findlater et al.[8]. They proposed a two-pixel stacked structure, using the Si depth to separate colors, but with the addition of color filters. Using a fairly complex 6T readout architecture, they fabricated a prototype sensor with cyan and yellow filters. A system with magenta and green filters over alternate pixels was also briefly discussed, but they did not develop it further. A similar device structure and readout circuit is described by Henker et al. for multi-channel CMOS sensors [11, 12]. Another architecture with blue and red stacked sensors in one pixel and green in a separate pixel has also been proposed [9]. The device structure and depth of the blue and red diodes is similar to Foveon's; but the middle, green-absorbing region is pulled out and placed in an adjacent pixel. No color filters are employed, relying on the absorption depth to separate the colors.

Recently [14], we proposed a modification to the standard Bayer CFA and photodiode structure for CMOS image sensors, which we call 2PFC$^{\text{TM}}$, for "Two Pixels, Full Color". It uses stacked blue and red sensors in one pixel and a single sensor in the adjacent green pixels. The difference from previous work [8–10] is that the device structure is completely compatible with standard CMOS processes, so fabrication costs, leakage, etc. should be low.

In the 2PFC$^{\text{TM}}$ pattern, the blue and red filters of the Bayer pattern are replaced by magenta filters (Fig. 1(e)), under which are two stacked, pinned photodiodes; the diode nearest the surface absorbs mostly blue light and the deeper diode absorbs mostly red light. Figure 2 is a schematic of a cross-section of the device. The overlying magenta filter absorbs

green light, improving color separation between the stacked diodes. A number of benefits naturally occur from these modifications. Higher well capacity, due to the thinner stacked diodes, leads to better dynamic range and signal-to-noise ratio. The reduction of color filters from three to two, while maintaining standard CMOS processing, keeps the overall cost similar to or less than one-color sensors.

Another advantage is that since the spatial resolution of green, red, and blue are identical, color aliasing is greatly reduced and luminance resolution is improved, at least for simple demosaicing schemes. Nyquist maps for Bayer and 2PFC^{TM} are compared in Figure 3. Bayer has higher Nyquist frequency in the horizontal and vertical directions than along the diagonal for green, while red and blue are the converse. In comparison, the green, red, and blue Nyquist frequencies are all identical for 2PFC^{TM} and are highest along the horizontal and vertical directions. This is highly desirable, since the resolution differences for Bayer increase color aliasing. Also, the human visual system has higher spatial resolution in the horizontal and vertical directions than along the diagonal direction. The Bayer CFA green matches the human eye 2D contrast sensitivity function (CSF), but red and blue do not. For the 2PFC^{TM} pattern, all three colors match the eye's CSF.

With the 2PFC^{TM} sensor, most of the digital processing steps are similar to those of a standard sensor. This includes white balancing, tone mapping, and color correction. However, demosaicing has to be adapted to the new CFA design. It should exploit the additional color information available per pixel location to produce better, less-aliased, and sharper full color images. In the next section, we review some state of the art demosaicing algorithms. In Section III, we describe adaptations of spatial and frequency-based demosaicing algorithms for 2PFC^{TM}. In Section IV, we compare the results from the best demosaicing methods for the Bayer CFA with our implementations for 2PFC^{TM}. Finally, a system performance analysis, including resolution and noise, is discussed in Section V.

II. REVIEW OF DEMOSAICING

In 2008, Li et al.[18] reviewed more than 70 papers on demosaicing techniques. They state that most methods follow a sequential approach. These start by interpolating the green channel, which has twice as many samples as the red and blue channels in a Bayer CFA. As the algorithms are sequential, errors in the green estimation propagate to the next

steps of reconstruction. Most of the effort is therefore put into green channel reconstruction. Next, the red and blue channels are interpolated, often using a less expensive algorithm. Finally, refinement steps are applied in order to improve the high frequency content of the image and remove artifacts. The state of the art demosaicing algorithms can be separated into two main classes: spatial domain approaches and frequency domain approaches.

A. Spatial Domain Approaches

In the spatial domain, the green channel is first reconstructed using an edge-directed technique [19–22]. Some algorithms first interpolate the green channel in several directions and then decide which direction to retain for each pixel [23–27]. Most use the assumption that color differences vary slowly in smooth regions [18] and interpolate the color difference instead of using only the green channel information.

Once the green channel is interpolated, red and blue are reconstructed using a simpler technique, such as bilinear interpolation of color differences [19, 22, 28–30]. The interpolation direction found in the previous step can also be used to improve the accuracy of the red and blue reconstruction [23, 31].

Most demosaicing algorithms include a refinement step, often exploiting correlation between high frequency captured information across color channels. As the color filter array spectral sensitivities usually overlap (Fig. 9), R, G, and B values are correlated. Since the visual system's chromatic contrast sensitivity function has a lower spatial frequency cutoff than the luminance contrast sensitivity function, high frequency captured information at green pixel locations is used to improve the reconstructed red and blue pixels to avoid color fringing [32].

B. Frequency Domain Approaches

Alleysson et al.[33] proposed a demosaicing method which directly exploits the multiplexing of color and luminance information by the sensor array. They showed that for a Bayer pattern, the CFA signal can be decomposed into full resolution luminance and modulated chrominance components. Fig. 5(a) shows for a Bayer CFA how the luminance and chrominance information are separated in a frequency domain representation. The lumi-

nance information is mostly located at lower frequencies (center), whereas the chrominance information is located at higher frequencies (borders and corners). This separation suggested demosaicing by first separating luminance from chrominance using linear filtering followed by reconstructing chrominance information via interpolation. The results of this method highly depend on the filter used to extract luminance and chrominance from the CFA. As there usually is non-negligible cross-talk between luminance and chrominance information, this method can result in reconstructed images exhibiting color aliasing and other artifacts. Alleysson et al.[33] described the four main types of artifacts as blurring, color aliasing, grid effect, and watercolor effect. Subsequently, Dubois [34] and Lian et al.[35] proposed enhancements that improved the results by adaptively filtering the luminance component. Recent research to improve these frequency-based methods has explored the design of non-Bayer CFA patterns to maximize the separation between luminance and chrominance information in the frequency domain, thus reducing cross-talk [17, 36, 37]. The CFA patterns considered all use single color (single-junction) photodetectors.

III. ADAPTATIONS OF DEMOSAICING METHODS TO 2PFC™

A. Adaptation of Spatial Demosaicing to 2PFC™

Existing spatial demosaicing algorithms can easily be adapted for 2PFC™, as the latter contains the same signal as Bayer *plus* additional red and blue data. Beyond applying the same demosaicing technique, the extra data can be used to improve both the directional interpolation and high-frequency refinement.

We adapted Menon et al.'s demosaicing with directional filtering and *a posteriori* decision [32] method to 2PFC™. This method was chosen as it provides good results for relatively low computational complexity. Our approach is illustrated in Figure 4(a). First, we perform a directional interpolation of the green channel along vertical and horizontal directions. We then compute a decision map to determine the best interpolation direction for each pixel. In a third step, we interpolate the red and blue channels by bilinear interpolation of color differences. Next, we perform a refinement step that improves the high frequency content of reconstructed pixels, as described in Section II A. Finally, median filtering of color differences can be applied to the output image to further reduce remaining artifacts

(see Section III B 3).

This method, adapted for 2PFC$^{\text{TM}}$, provides very good results (see Section IV). However, the method was not designed with 2PFC$^{\text{TM}}$ in mind and therefore does not take full advantage of the new sensor geometry. Therefore, we will not provide more details on the method and will concentrate on our frequency-based demosaicing algorithm developed in Section III B.

B. Frequency Analysis of 2PFC$^{\text{TM}}$ [G R/B] Pattern

Using Dubois' notations [34], we can analyze the frequency representation of the 2PFC$^{\text{TM}}$ CFA pattern. Since red and blue pixels are overlapping within 2PFC$^{\text{TM}}$, we consider two mosaiced patterns: one [G R] and one [G B] pattern (pattern of Fig. 1(e) but replacing magenta by red and blue, respectively). The derivation will be done only for [G R] as it is identical for [G B].

Let $f_G[n,m]$ and $f_R[n,m]$ represent the green and red channels of the original image and $f_{CFA}[n,m]$ the output of our 2PFC$^{\text{TM}}$ sensor at pixel location $[n,m]$. $f_{CFA}[n,m]$ is obtained by sub-sampling the $f_G[n,m]$ and $f_R[n,m]$ functions to match the [G R] CFA pattern. The sub-sampling can be represented as a multiplication by the functions $m_i[n,m]$, $i \in \{G,R\}$ that take value 1 or zero:

$$\begin{aligned} m_G[n,m] &= \frac{1}{2}(1+(-1)^{n+m}), \\ m_R[n,m] &= \frac{1}{2}(1+(-1)^{n+m+1}). \end{aligned} \tag{1}$$

With these modulation functions, the CFA signal $f_{CFA}[n,m]$ can be written as

$$f_{CFA}[n,m] = \frac{1}{2}f_G[n,m](1+(-1)^{n+m}) + \frac{1}{2}f_R[n,m](1+(-1)^{n+m+1}). \tag{2}$$

Equation 2 can be rewritten as

$$\begin{aligned} f_{CFA}[n,m] &= \frac{1}{2}\left[f_G[n,m]+f_R[n,m]\right] + \frac{1}{2}(-1)^{n+m}\left[f_G[n,m]-f_R[n,m]\right] \\ &:= f_L[n,m] + f_C[n,m](-1)^{n+m}, \end{aligned} \tag{3}$$

where f_L is a fully sampled signal associated with luminance and f_C is a modulated signal defined as chrominance.

Noting that $-1 = exp(j\pi)$ and defining the discrete time Fourier transform (DTFT) as

$$F(u,v) = \sum_{n\in\mathbb{Z}} \sum_{m\in\mathbb{Z}} f[n,m] e^{-j2\pi un} e^{-j2\pi vm}, \tag{4}$$

we can rewrite Equation 3 as

$$f_{CFA}[n,m] = f_L[n,m] + f_C[n,m] \exp\left(j2\pi(n+m)/2\right) \tag{5}$$

and taking its DTFT yields

$$F_{CFA}(u,v) = F_L(u,v) + F_C(u-0.5, v-0.5). \tag{6}$$

The same result is obtained for the [G B] pattern by replacing R by B in the above equations. Comparing this result with that of the Bayer pattern, we first note that 2PFC$^{\text{TM}}$ has its luminance/chrominance information split into two Fourier spectra instead of one with the Bayer CFA, as we consider two sub-mosaic: [G R] and [G B]. While the Bayer CFA has chrominance located at corners and borders of the Fourier spectrum, each Fourier image of the 2PFC$^{\text{TM}}$ sub-mosaic has chrominance located only at the corners, i.e. at high frequencies, thus maximizing the separation between luminance and chrominance (Fig. 5). The location of the chrominance and the small amount of cross-talk permit the usage of a simpler separation filter than those used for a Bayer CFA. An example of a filter and its frequency response is given in Fig. 6.

1. Filter Design

In our proposed demosaicing algorithm, we use a filter h_L to extract luminance from the CFA image (Eq. 7). The filter was computed by defining a standard least-squares problem [39]

$$h_L = \arg\min_h E[(f_L - h * f_{CFA})^2],$$

where f_{CFA} is the CFA image, f_L the luminance image, and h the extraction filter to optimize. In practice, the error is minimized over a training set of full color images and f_L is thus known. h_L can be computed for any filter size. We used a 5x5 and 21x21 filter for the experiments (Section IV).

The luminance extraction filter h_L was estimated using the commonly-used 24 Kodak RGB image set [38]. When implemented in a full digital camera workflow, the filter will

need to be re-computed based on sensor data to account for the effect of the color filter spectral sensitivities [40].

2. Proposed Demosaicing Algorithm

A block diagram of our approach is shown in Figure 4(b). With the 2PFC$^{\text{TM}}$ CFA, the red and blue color samples have the same spatial location. The single channel CFA image is separated into two channels ([G R] and [G B]) that are processed in parallel and recombined at the end of the process to form a single RGB color image.

Let f_{CFA}^{GR} and f_{CFA}^{GB} be the two above-mentioned mosaiced channels and h_L the luminance extraction filter described in Section III B 1. In a first step, h_L is applied to f_{CFA}^{GR} and f_{CFA}^{GB}, respectively. The extracted luminances can be written as

$$\begin{aligned} f_L^{GR} &= h_L * f_{CFA}^{GR}, \\ f_L^{GB} &= h_L * f_{CFA}^{GB}. \end{aligned} \tag{7}$$

Note that we have two "luminance" components, f_L^{GR} and f_L^{GB}. They differ from the *real* luminance, which is unique. Both f_L^{GR} and f_L^{GB} are extracted from a channel ([G R] or [G B]) where a part of the spectrum is missing (blue or red). These extracted luminances thus correspond only to a partial luminance signal and will be combined later to recover the full luminance.

The chrominance part is retrieved by subtracting the above luminances from the CFA signals:

$$\begin{aligned} f_C^{GR} &= f_{CFA}^{GR} - f_L^{GR}, \\ f_C^{GB} &= f_{CFA}^{GB} - f_L^{GB}. \end{aligned} \tag{8}$$

The green channel is handled differently as it is present in both f_{CFA}^{GR} and f_{CFA}^{GB}. The luminance and chrominance are defined as the average of the values extracted from the two channels, such as

$$\begin{aligned} f_L^{GM} &= (f_L^{GR} + f_L^{GB})/2, \\ f_C^{GM} &= (f_C^{GR} + f_C^{GB})/2. \end{aligned} \tag{9}$$

Taking the average is equivalent to considering a [G M] channel and applying Eq. 7 and 8, where M is magenta, i.e. the combination of red and blue.

Let $L = \{f_L^{GR}; f_L^{GM}; f_L^{GB}\}$ be the 3-channel extracted luminance and $C = \{f_C^{GR}; f_C^{GM}; f_C^{GB}\}$ be the 3-channel multiplexed chrominances. Each chrominance channel in C is de-multiplexed according to the CFA pattern and the missing values are reconstructed using bilinear interpolation to form $\hat{C}$. A more sophisticated interpolation algorithm would not produce much better results due to the human visual system's lower sensitivity to high chrominance frequency content.

Finally, the full RGB color image $\hat{f}$ is reconstructed by adding the chrominance channels to their respective luminance channels:

$$\hat{f} = L + \hat{C}. \tag{10}$$

3. Median Filtering

The reconstructed image might still contain artifacts, as small amounts of cross-talk often exist between luminance and chrominance in the Fourier space. To reduce artifact visibility, we perform a median filtering on color differences. Using the assumption that color differences vary slowly, small variations in color are suppressed by median filtering. Our median filtering is computed using a 3×3 kernel and is applied only on the reconstructed pixels, whereas it is applied on all pixels in other approaches [27]. The R channel is computed first, followed by the B and finally the G channel:

1. $R = G + median(R - G)$
2. $B = G + median(B - G)$
3. $G = \frac{1}{2}[R + median(R - G) + B + median(B - G)]$

Median filtering can be applied more than once, but we found that the benefit of a second median filtering is generally not worth the computational cost.

IV. EXPERIMENTS

In this section, we present experimental results from several demosaicing algorithms applied to the Bayer CFA and the 2PFC$^{\text{TM}}$ CFA. The Bayer CFA algorithms were chosen based on performance and on availability of a reference implementation, and are: Bilinear

interpolation, Lian et al.'s adaptive filtering (AF) [35], Zhang and Wu's DLMMSE (DL) [25], Gunturk et al.'s alternating projections (POCS) [41], Menon and Calvagno's wavelet based method (DBW) [42], and Menon et al.'s directional filtering (DFPD) [32]. The 2PFC^{TM} CFA algorithms are: Bilinear interpolation, the directional-spatial interpolation (S) described in Section III A, and frequency-based filtering with 5×5 (F5) and 21×21 (F21) filters as described in Section III B 1 and III B 2. In Table I, some algorithms' names are followed by a + sign, which indicates that median filtering, as described in Section III B 3, was employed as a post-processing step.

The algorithms were applied to the 24 Kodak PhotoCD images [38] after sub-sampling according to the CFAs. Sample results can be seen in Fig. 7. The metrics reported in Table I are computed after removing a 5-pixel border from each image in order to discount errors, since not all implementations take care of proper border reconstruction. The metrics used are color PSNR, S-CIELab ΔE color difference [43], and Lu and Tan's zipper artifact metric [23]. Zipper-like artifacts usually appear as alternating patterns in smooth regions near edges. The zipper effect is an increase in color difference with respect to its most similar neighboring pixel. The computation of zipper artifacts uses this observation. When the computed absolute color difference is bigger than a threshold, the pixel is considered to have a noticeable artifact. The threshold was set to 2.3 based on [23]. The zipper effect is expressed as a percentage of the total pixel number.

The metrics are computed not only on the full demosaiced image, but also separately for the smooth and edge regions of the reconstructed image, using Lu and Tan's [23] procedure to separate the image content using a low-pass filter. As high-frequency regions are the most difficult parts to reconstruct, the difference between algorithms should be noticeable in the edge image.

The metrics in Table I first show that demosaicing algorithms for 2PFC^{TM} CFA outperform those for Bayer CFA. Our frequency-based demosaicing method also performs very well compared to more complex spatial methods. PSNR is more than 4dB higher for 2PFC^{TM} than for Bayer CFA, whereas the difference is usually less than 1dB when comparing among state-of-the-art demosaicing algorithms. The spatial color difference is almost half, and the zipper effect is up to three time smaller for 2PFC^{TM} than Bayer CFA. These results are valid for both edge and smooth image regions. As expected, smooth regions are better reconstructed than edge regions for all algorithms, and methods for the 2PFC^{TM} CFA perform

	Full Image			**Smooth Image**			**Edge Image**		
	PSNR	ΔE	Zip	PSNR	ΔE	Zip	PSNR	ΔE	Zip
[B] Bilinear	30.22	1.70	35.43	34.48	1.38	29.04	22.92	8.58	77.64
[B] AF	39.60	0.82	3.43	41.53	0.80	2.14	34.29	3.15	9.99
[B] DL	40.03	0.79	2.96	41.96	0.76	1.86	34.71	3.09	8.99
[B] POCS	39.26	0.90	2.76	41.14	0.87	1.73	34.00	3.44	8.60
[B] DBW	39.68	0.84	3.33	41.68	0.82	1.95	34.32	3.22	10.85
[B] DFPD	39.28	0.88	5.01	41.26	0.84	3.42	33.91	3.34	13.51
[B] DFPD+	39.62	0.86	2.85	41.56	0.82	1.77	34.30	3.36	8.79
[2] Bilinear	33.21	1.08	35.38	37.28	0.93	30.02	26.00	4.90	73.07
[2] S	43.25	0.57	3.98	45.06	0.56	2.57	38.09	2.17	11.91
[2] S+	44.11	0.55	1.20	45.80	0.53	0.62	39.10	2.15	4.67
[2] F5	43.88	0.51	2.07	45.79	0.50	1.14	38.56	2.04	7.31
[2] F21	44.25	0.49	1.34	46.05	0.47	0.70	39.08	1.96	5.10
[2] F5+	44.33	0.52	1.10	46.08	0.50	0.56	39.22	2.09	4.31
[2] F21+	44.46	0.50	1.01	46.20	0.48	0.52	39.38	2.04	3.98

TABLE I: PSNR(dB), S-CIELab ΔE, and zipper effect (%) metrics of different demosaicing algorithms for [B] Bayer and [2] 2PFC^{TM} CFA on the Kodak PhotoCD image set [38]. Each metric is computed for the full image, smooth regions, and edge regions.

better than methods for the Bayer CFA. Additionally, median filtering of color differences greatly reduces zipper artifacts for any demosaicing method.

In our frequency-based algorithm, we use a filter to extract luminance from the 2PFC^{TM} CFA signal. We tested a wide range of filter sizes. Table I shows the results when using a 5x5 (F5) and a 21x21 (F21) filter. Using a 5x5 filter does not penalize results much compared to a larger 21x21 filter. A small filter is sufficient as the luminance and chrominance are well separated in the Fourier space and, unlike with a Bayer CFA, chrominance is located only at the corners of the Fourier spectrum.

The advantages of using a 2PFC^{TM} CFA as opposed to a Bayer CFA are illustrated in Fig. 7. The reduction of color aliasing and zipper artifacts are clearly visible on all test images.

Kriss proposed a method for evaluating the potential for aliasing based on the system MTF [44]. As an additional evaluation criterion, we propose an alternative method to estimate the potential for color artifacts. A random grayscale image is generated, then subsampled according to the CFA pattern and finally demosaiced (Fig. 8). The use of a random image breaks the spatial correlation between neighboring pixels. Demosaicing methods, which extensively use those correlations, have a *worst case scenario* to process. The color aliasing that is produced is therefore a *potential for aliasing* (PA) [44]. It is measured by computing the S-CIELab color difference [43] between the original and the demosaiced image. Table II shows that 2PFC^{TM} has less potential for color aliasing. It should also be noted that median filtering of color differences helps to reduce aliasing.

Method	*PA (mean ΔE)*
[B] Bilinear	20.25
[2] Bilinear	17.34
[B] DFPD+	11.77
[2] S+	8.61
[2] F21	10.18
[2] F21+	8.60

TABLE II: Potential for color aliasing computed with several demosaicing methods for Bayer and 2PFC^{TM} CFAs.

This method for estimating the potential for aliasing of a demosaicing algorithm coupled with a CFA pattern, however, is far from perfect: the use of a grayscale image does not take into account color aliasing occurring at color edges or in color textured regions.

V. SYSTEM PERFORMANCE ANALYSIS

Images produced with a 2PFC^{TM} CFA are less prone to demosaicing artifacts than images produced with a Bayer CFA. However, the quality of 2PFC^{TM}-based images must be estimated on a full digital camera pipeline and not only on the demosaicing process. We used the Image Systems Evaluation Tools (ISET [45]) to simulate a full digital camera workflow and compare the performance of Bayer-based versus 2PFC^{TM} sensors.

ISET is composed of several Matlab modules that control the different stages of image acquisition and processing. These stages comprise the scene, optics, the sensor, and the post-processing. The scene can be a multispectral image, a RGB image, or a generated test target. Default optics were used. The sensor and pixel parameters are set with appropriate values, including noise parameters. Post-processing includes demosaicing, white-balancing, and color-matrixing. The goal being to compare Bayer and 2PFC^{TM}, most of the parameters are kept the same for the two sensors, including optics, pixel characteristics, noise parameters, and color post-processing. The main difference, besides the CFA pattern, is the color filter set used and its effect on the post-processing steps. For the Bayer-based sensor, we used generic RGB filters provided by ISET (ISET RGB) and color filters from a professional digital camera (C-RGB). For 2PFC^{TM}, we used two filter sets obtained by optical simulation, called *2PFC-A* and *2PFC-B*, respectively [14]. These explore a range of possible relative RGB sensitivities. Due to the nature of the stacked blue and red diodes, there is some color mixing between these channels, the extent of which depends on the optical and electrical design of the sensor. The two filter sets are intended to test the effect of spectra variation. The four filter sets' spectral sensitivity responses are plotted in Figure 9.

A. Resolution

In terms of spatial resolution, a 2PFC^{TM} stacked sensor can be expected to have slightly better performance than a Bayer array at the same pixel pitch. But the expected difference may not be large and also strongly depends on the demosaicing method. To evaluate the Bayer and 2PFC^{TM} resolution performance, we analyzed simulated images of the ISO12233 slanted bar target [46] and report MTF50 values, i.e. the frequency at which the modulated transfer function value is half of its DC value. Fig. 10 presents the derived MTF curves for the R, G, and B channels. The black curve represents the luminance MTF response. For bilinear demosaicing (Fig. 10(a) and (b)), 2PFC^{TM} performs better than Bayer in terms of MTF50 values and the R, G, and B MTF curves are coincident. However, when using state-of-the-art demosaicing algorithms, the resolution difference as measured by the MTF becomes much smaller. Fig. 10 compares Menon et al.'s method [32] with our frequency-based 2PFC^{TM} demosaicing. Both give similar, much higher MTF50 values than the bilinear cases. Also, the Menon et al. method does quite well for this black-and-white edge at

equating the MTF responses of the R, G, and B channels (mainly due to how it equates the high frequency content between R, G, and B channels), while 2PFC^{TM} exhibits some spread. Thus, using a more-sophisticated Bayer demosaicing method leads to a much sharper resulting image and with resolution comparable to that of a 2PFC^{TM} image. 2PFC^{TM} can, therefore, be considered to have higher resolution only when using low-complexity Bayer demosaicing. This slanted-bar resolution measure, however, does not necessarily indicate which demosaicing method is of better quality as Bayer tends to have more color artifacts than 2PFC^{TM} (e.g. see Fig. 7).

We also evaluated resolution using a method stipulated by the Camera & Imaging Products Association (CIPA) [47]. With ISET, we simulated images of the J1 region of the ISO12233 test chart as if the chart were 100cm from the camera (Fig. 11). These images were then input into the "HYRes" software downloaded from the CIPA website. This software analyzes the images and determines the point at which the 5 lines in the J1 test pattern become unresolved, indicated by the red line in each image. Fig. 11 shows Bayer images for bilinear, and Menon et al. demosaicing, and 2PFC^{TM} with bilinear, spatial, and frequency-based demosaicing. The calculated resolution is 135 lines/picture-height (l/ph) for Bayer with bilinear demosaicing, but improves dramatically to 175 l/ph for all the rest, including 2PFC^{TM} with bilinear demosaicing.

B. Noise

ISET simulates several noise sources, including dark current, read noise, dark signal non-uniformity (DSNU), and photo response non-uniformity (PRNU). Noise parameters are held constant for Bayer-based and 2PFC^{TM} sensors simulations as we do not yet have an accurate noise model of the 2PFC^{TM} sensor, nor a prototype to measure it. The main source of noise level difference in the simulated results comes from the different color filters spectral sensitivity response and from the color matrixing to transform camera RGB values to a standard color space. The spectral sensitivity curves of 2PFC^{TM} filters (Fig. 9) are more correlated as the wavelength separation for the stacked pixel is not perfect and some reddish (respectively bluish) light is captured in the blue (respectively red) sensitive area of the pixel. The two 2PFC^{TM} spectral sensitivity curves shown in Figure 9 represent a range of possible curves [14] to explore the effect of this variation.

Let M be the transformation matrix from camera RGB (cRGB) to sRGB values. M can be written as $M = M_s \cdot M_c$, where M_c is the transformation matrix from cRGB to XYZ and M_s is the transformation matrix from XYZ to sRGB. The values of M_c depend on the overall sensor spectral sensitivities and on the method used to compute it. M_s is fixed and defined by the sRGB standard [48]. Let κ be the condition number of M. In the case of the linear color transform M, κ is computed as the ratio of maximum to minimum singular value and indicates how much the transformation is sensitive to noise [49]. A perfect value of κ is unity and indicates an identity operation. Larger values of κ indicate larger noise amplification in general. We computed κ for the four different filter sets of Figure 9 (Tab. III): two used with the Bayer CFA (ISET RGB and C-RGB) and two used with the 2PFC$^{\text{TM}}$ CFA (2PFC-A and 2PFC-B). M_c was computed using the white point preserving least square method [50].

	ISET RGB	C-RGB	2PFC-A	2PFC-B
κ	1.65	1.89	2.07	1.90
M	$\begin{pmatrix} 0.602 & 0.250 & 0.148 \\ 0.284 & 0.649 & 0.067 \\ 0.067 & -0.018 & 0.952 \end{pmatrix}$	$\begin{pmatrix} 0.632 & 0.186 & 0.182 \\ 0.311 & 0.723 & -0.034 \\ 0.062 & -0.123 & 1.061 \end{pmatrix}$	$\begin{pmatrix} 0.665 & 0.241 & 0.094 \\ 0.376 & 0.625 & -0.001 \\ -0.260 & 0.018 & 1.242 \end{pmatrix}$	$\begin{pmatrix} 0.629 & 0.211 & 0.160 \\ 0.258 & 0.734 & 0.008 \\ -0.089 & 0.054 & 1.035 \end{pmatrix}$

TABLE III: Condition number κ of the linear transformation M from cRGB to sRGB for 4 different filter sets.

The condition number when using filters for 2PFC$^{\text{TM}}$ is slightly higher than for Bayer-based sensor filters. The ISET RGB filter set is, however, an ideal case. Comparing real filters (C-RGB) to 2PFC$^{\text{TM}}$ filter sets, the difference becomes much smaller.

If we consider the worst case scenario, the color noise should be more amplified with 2PFC$^{\text{TM}}$ than with Bayer-based sensors when converting from cRGB to sRGB and using the same method to compute M_c. To verify our hypothesis, signal to noise ratio (SNR) was measured on the 18% gray level patch from a simulated Macbeth color checker under D65 rendered with ISET to sRGB (Fig. 12). The SNR is computed for both luma Y and chroma CbCr of the YCbCr color space. Figure 13 shows the variation of SNR with exposure time for all four filter sets. At low exposures, luma noise is lower for 2PFC$^{\text{TM}}$ than for Bayer. A justification can be found in the higher quantum efficiency of the 2PFC$^{\text{TM}}$ color filters spectral sensitivities response. As expected, chroma noise is slightly higher for 2PFC$^{\text{TM}}$.

Sensitivity to noise can vary by modifying how M_c is computed. Vora and Herley [49]

showed that there is a trade-off between color saturation and noise sensitivity. With 2PFC^{TM} sensors having more correlated filters than Bayer-based sensors, the colors tend to be less saturated. In order to achieve the desired noise behavior, M_c can be modified at the expense of color saturation.

VI. CONCLUSION

We have presented a modification to the standard single color CFA and photodiode structure for CMOS image sensors called 2PFC^{TM} (Two Pixels, Full Color). This new stacked sensor has only two color filters (green and magenta) to capture three colors (red, green, and blue). Green is captured with a standard diode overlaid by a green filter, while red and blue are captured by stacked diodes overlaid by a magenta filter. Thus, the sampling frequency for the three channels (R, G, and B) is identical.

The new 2PFC^{TM} geometry requires a new demosaicing method to reconstruct the full color image. We developed a frequency-based demosaicing algorithm adapted for the new CFA design. Our approach uses the separation of luminance and chrominance in the Fourier domain of the CFA to reconstruct missing color pixels. Unlike methods for single color CFA sensors, luminance and chrominance are well separated in the Fourier domain, which enables the use of computationally inexpensive linear filters.

The demosaicing algorithm shows excellent performance compared to methods for the Bayer CFA in terms of color PSNR, spatial color difference S-CIELab ΔE, and zipper artifacts. Color aliasing is also greatly reduced, both visually and also according to our proposed method that can estimate the potential for aliasing of demosaicing algorithms.

When integrated in a full system simulation, 2PFC^{TM} visually still performs better than Bayer. We evaluated resolving power using two methods: MTF50 computed on a slanted edge and the CIPA method. Resolution is the same for computationally expensive Bayer demosaicing algorithms and less expensive 2PFC^{TM} methods. When analyzing noise, however, we noticed that the chroma noise is slightly higher with 2PFC^{TM} as the color filters' spectral sensitivities are more correlated than with Bayer. A better noise model of 2PFC^{TM} is, however, necessary to get a more precise understanding of the difference between Bayer-based and 2PFC^{TM} sensor noise.

The device structure of the 2PFC^{TM} is compatible with standard CMOS processes. We

therefore believe that it is possible, at equivalent cost, to use the same production methods to fabricate a sensor that is better than existing ones in term of image quality or, alternatively, produce a sensor with an equivalent image quality but with computationally less expensive algorithms for use in smaller devices such as cell phones.

More information on the 2PFC^{TM} imager is available at http://www.sharplabs.com/2pfc.php.

Acknowledgments

The authors would like to thank S. Süsstrunk and M.A. Kriss for their helpful comments, and D. Menon and B.K. Gunturk for providing the code to their algorithms. This work was supported in part by the Swiss National Science Foundation under grant number 200021-113829.

---

[1] B. E. Bayer, "Color imaging array." U.S. Patent 3 971 065, 1976.

[2] W. N. Carr, "Multi-spectrum photodiode devices." US Patent 4 238 760, 1980.

[3] N. Harada and O. Yoshida, "Visible/infrared imaging device with stacked cell structure." US Patent 4 651 001, 1987.

[4] P. Seitz, D. Leipold, J. Kramer, and J. M. Raynor, "Smart optical and image sensors fabricated with industrial cmos/ccd semiconductor processes," in *Proc. SPIE*, **1900**, 1993.

[5] R. B. Merrill, "Color separation in an active pixel cell imaging array using a triple-well-structure." US Patent 5 965 875, 1999.

[6] D. L. Gilblom, S. K. Yoo, and P. Ventura, "Operation and performance of a color image sensor with layered photodiodes," in *Proc. of SPIE*, **5074**, pp. 318–331, 2003.

[7] P. M. Hubel, J. Liu, and R. J. Guttosch, "Spatial frequency response of color image sensors: Bayer color filters and foveon x3," in *Proc. of SPIE*, **5301**, pp. 402–407, 2004.

[8] K. M. Findlater, D. Renshaw, J. E. D. Hurwitz, R. K. Henderson, M. D. Purcell, S. G. Smith, and T. E. R. Bailey, "A cmos image sensor with a double-junction active pixel," *IEEE Transaction on Electron Devices* **50**, pp. 32–42, January 2003.

[9] S. C. Hong, "CMOS image sensor and method of fabrication." U.S. Patent 6 946 715, 2005.

[10] T. Saito and T. Komatsu, "Image recovery for a direct color imaging approach using a color filter array," in *IS&T/SPIE Electronic Imaging: Digital Photography II*, **6069**, 2006.

[11] S. Henker, J.-U. Schlüßler, and R. Schüffny, "Concept of color correction on multi-channel cmos sensors," in *Digital Image Computing: Techniques and Applications, 7th Biennial Australian Pattern Recognition Society Conference - DICTA*, **2**, pp. 771–780, 2003.

[12] S. Henker, C. Mayr, J.-U. Schlüßler, R. Schüffny, U. Ramacher, and A. Heittmann, "Active pixel sensor arrays in 90/65nm cmos-technologies with vertically stacked photodiodes," in *International Image Sensor Workshop*, 2007.

[13] H. Steibig, R. A. Street, D. Knipp, M. Krause, and J. Ho, "Vertically integrated thin-film color sensor arrays for advanced sensing applications," *Appl. Phys. Lett.* **88**, 2006.

[14] D. J. Tweet, J. J. Lee, J. M. Speigle, and D. Tamburrino, "2PFC image sensors: better image quality at lower cost," in *IS&T/SPIE Electronic Imaging: Digital Photography V*, **7250**, 2009.

[15] R. Lukac and K. N. Plataniotis, "Color filter arrays: Design and performance analysis," *IEEE Trans. Consumer Electron.* **51**, pp. 1260–1267, 2005.

[16] T. Kijima, H. Nakamura, J. T. Compton, and J. F. Hamilton Jr., "Image sensor with improved light sensitivity." U.S. Patent Application 20 070 177 236, 2007.

[17] K. Hirakawa and P. J. Wolfe, "Second-generation color filter array and demosaicking designs," in *Proc. SPIE*, **6822**, p. 68221P, 2008.

[18] X. Li, B. Gunturk, and L. Zhang, "Image demosaicing: A systematic survey," in *IS&T/SPIE Electronic Imaging: Visual Communications and Image Processing*, **6822**, 2008.

[19] J. E. Adams and J. F. Hamilton Jr., "Adaptive color plane interpolation in single color electronic camera." U.S. Patent 5 506 619, 1996.

[20] R. H. Hibbard, "Apparatus and method for adaptively interpolating a full color image utilizing luminance gradients." U.S. Patent 5 382 976, 1995.

[21] J. F. Hamilton Jr. and J. E. Adams, "Adaptive color plane interpolation in single color electronic camera." U.S. Patent 5 629 734, 1997.

[22] C. Laroche and M. Prescott, "Apparatus and method for adaptively interpolating a full color image utilizing chrominance gradients." U.S. Patent 5 373 322, 1994.

[23] W. Lu and Y.-P. Tan, "Color filter array demosaicking: new method and performance measures.," *IEEE Transactions on Image Processing* **12**(10), pp. 1194–1210, 2003.

[24] X. Wu and N. Zhang, "Primary-consistent soft-decision color demosaicking for digital cameras

(patent pending)," *IEEE Transactions on Image Processing* **13**, pp. 2163–1274, September 2004.

[25] L. Zhang and X. Wu, "Color demosaicking via directional linear minimum mean square-error estimation," *IEEE Trans. Image Processing* **14**, pp. 2167–2178, December 2005.

[26] C.-Y. Tsai and K.-T. Song, "Heterogeneity-projection hard-decision color interpolation using spectral-spatial correlation," *IEEE Transactions on Image Processing* **16**(1), pp. 78–91, 2007.

[27] K. Hirakawa and T. W. Parks, "Adaptive homogeneity-directed demosaicing algorithm," *IEEE Trans. Image Processing* **14**(3), pp. 360–369, 2005.

[28] D. Cok, "Signal processing method and apparatus for producing interpolated chrominance values in a sampled color image signal." U.S. Patent 4 642 678, 1987.

[29] W. T. Freeman, "Method and apparatus for reconstructing missing color samples." U.S. Patent 4 774 565, September 1988.

[30] S. Pei and I. Tam, "Effective color interpolation in ccd color filter array using signal correlation," *CirSys Video* **13**(6), pp. 503–513, 2003.

[31] C. Yuk, O. Au, R. Li, and S.-Y. Lam, "Color demosaicking using direction similarity in color difference spaces," in *International Symposium on Circuits and Systems*, pp. 1281–1284, 2007.

[32] D. Menon, S. Andriani, and G. Calvagno, "Demosaicing with directional filtering and a posteriori decision," *IEEE Transactions on Image Processing* **16**(1), pp. 132–141, 2007.

[33] D. Alleysson, S. Süsstrunk, and J. Hérault, "Linear demosaicing inspired by the human visual system," *IEEE Transactions on Image Processing* **14**(4), pp. 439–449, 2005. Supplementary material available at: http://ivrg.epfl.ch/supplementary_material/index.html.

[34] E. Dubois, "Frequency-domain methods for demosaicking of bayer-sampled color images," *IEEE Signal Processing Letters* **12**, pp. 847–850, December 2005.

[35] N. Lian, L. Chang, and Y.-P. Tan, "Improved color filter array demosaicking by accurate luminance estimation.," in *Proc. IEEE International Conference on Image Processing ICIP 2005*, pp. 41–44, 2005.

[36] D. Alleysson and B. Chaix de Lavarène, "Frequency selection demosaicking: A review and a look ahead," in *IS&T/SPIE Electronic Imaging: Visual Communications and Image Processing*, **6822**, 2008.

[37] Y. M. Lu and M. Vetterli, "Optimal color filter array design: Quantitative conditions and an efficient search procedure," in *Proc. SPIE Conference on Digital Photography V*, **7250**, 2009.

[38] "Kodak photocd image database." http://r0k.us/graphics/kodak/.

[39] E. Dubois, "Filter design for adaptive frequency-domain bayer demosaicking," in *Proc. IEEE International Conference on Image Processing ICIP 2006*, 2006.

[40] D. Alleysson, S. Süsstrunk, and J. Marguier, "Influence of Spectral Sensitivity Functions on color demosaicing," in *IS&T/SID 11th Color Imaging Conference*, **11**, pp. 351–357, 2003.

[41] B. K. Gunturk, Y. Altunbasak, and R. M. Mersereau, "Color plane interpolation using alternating projections.," *IEEE Transactions on Image Processing* **11**, pp. 997–1013, September 2002.

[42] D. Menon and G. Calvagno, "Demosaicing based on wavelet analysis of the luminance component," in *Proc. IEEE International Conference on Image Processing ICIP 2007*, pp. 181–184, IEEE, 2007.

[43] X. Zhang and B. A. Wandell, "A spatial extension of cielab for digital color image reproduction," in *Proceedings of the SID Symposiums*, pp. 731–734, 1996.

[44] M. A. Kriss, "Tradeoff between aliasing artifacts and sharpness in assessing image quality," in *Image Processing, Image Quality, Image Capture, Systems Conference PICS*, pp. 247–256, 1998.

[45] J. E. Farrell, F. Xiao, P. B. Catrysse, and B. A. Wandell, "A simulation tool for evaluating digital camera image quality," in *IS&T/SPIE Electronic Imaging*, 2003.

[46] "Photography – Electronic still-picture cameras – Resolution measurements." ISO12233, 2000.

[47] "CIPA DC-003-Translation-2003, resolution measurement methods for digital cameras." Camera and Imaging Products Association (CIPA), 2003.

[48] "IEC 61966 2-1:1999. multimedia systems and equipment - colour measurment and management - part 2-1: colour management-default RGB colour space - sRGB," 1999.

[49] P. Vora and C. Herley, "Trade-offs between color saturation and noise sensitivity in image sensors," in *Proc. IEEE Int. Conf. Image Processing*, **1**, pp. 196–200, 1998.

[50] G. D. Finlayson and M. S. Drew, "Constrained least-squares regression in color spaces," *Journal of Electronic Imaging* **6**, pp. 484–493, October 1997.

Daniel Tamburrino has received his MS in physics from the Ecole Polytechnique Fédérale de Lausanne (EPFL) in 2003. He worked two years on an e-learning project about scientific and forensic photography. Since 2006, he has been a Research Assistant in the Image and Visual Representation Group at EPFL. In 2008, he visited Sharp Labs of America, Camas, WA, as an intern.

Jon Speigle is a researcher at the Sharp Laboratories of America, where he has worked on color science, image enhancement algorithms, and image quality evaluation for print, scan, and display applications. He received his BS degree in aeronautical engineering from the Massachusetts Institute of Technology with a specialization in avionics. In 1997 he received his PhD in Psychology from the University of California, Santa Barbara, focusing on visual perception and psychophysics. His current interests are in color imaging, image quality modeling, and the application of spatiotemporal visual models to video enhancement algorithms.

Doug Tweet is a Principal Engineer at Sharp Labs of America, where he has worked on CMOS image sensors and germanium IR detectors, as well as strained silicon and SiGe CMOS transistors. He received his Ph.D. in Physics from the University of Washington in 1990. Before joining Sharp in 1997 he worked in Japan for NEC and the Electrotechnical laboratory.

Jong-Jan Lee is a Principal Research Scientist at the Sharp Laboratories of America. He received his PhD from Arizona State University in 1994 and worked for Sharp Microelectronics Technology, WaferTech and Motorola before joined SLA in 2001. His has broad experience in the IC industry, including ESD protection device design, 1T FRAM device, strained silicon on insulator devices, and CMOS and CCD imagers. He has more than 20 journal publications and 77 patents.

FIG. 1: CFA patterns: (a) Bayer [1], (b) Lukac [15], (c) Kodak [16], (d) Hirakawa's "Pattern A" [17] and (e) 2PFC$^{\mathrm{TM}}$[14].

FIG. 2: Device structure of 2PFC$^{\mathrm{TM}}$.

FIG. 3: Nyquist spatial frequency limits for (a) Bayer and (b) 2PFC$^{\mathrm{TM}}$ in the horizontal and vertical directions. f_h and f_v are the spatial frequencies in the horizontal and vertical direction, respectively.

FIG. 4: Block diagrams of (a) spatial-based demosaicing (Section III A) and (b) frequency-based demosaicing (Section III B 2).

FIG. 5: Mean representation of the log magnitude of the Fourier transform for the 24 kodak images [38] with (a) Bayer CFA: chrominance is located at borders and corners, (b) 2PFC$^{\mathrm{TM}}$ [G R] CFA: chrominance is located at corners only.

FIG. 6: (a) 5×5 filter used to extract luminance from the 2PFC$^{\mathrm{TM}}$ CFA and (b) its frequency response.

FIG. 7: Zoom-in of a cropped part of the Kodak *Lighthouse* image after demosaicing: (a) Original image, (b) [Bayer] bilinear, (c) [Bayer] adaptive filtering (AF) [35], (d) [Bayer] DLMMSE (DL) [25], (e) [Bayer] POCS [41], (f) [Bayer] DBW [42], (g) [Bayer] DFPD [32], (h) [2PFC] bilinear, (i) [2PFC] Spatial method, (j) [2PFC] Spatial method w/ median filtering, (k) [2PFC] Frequency-based method with 5x5 filter, and (l) [2PFC] Frequency-based method with 5x5 filter and median filtering.

FIG. 8: Potential for aliasing metric. (a) Random grayscale image, (b) Bayer CFA demosaicing showing multi-colored arifacts, and (c) 2PFC$^{\mathrm{TM}}$ CFA demsaicing showing green-magenta color artifacts.

FIG. 9: Sensor spectral sensitivity response and quantum efficiency for (a) generic ISET RGB filters, (b) C-RGB filters (c) 2PFC$^{\mathrm{TM}}$ *2PFC-A* filters, and (d) 2PFC$^{\mathrm{TM}}$ *2PFC-B* filters.

FIG. 10: R, G, B, and luminance modulation transfer function (MTF) curves of simulated system after demosaicing for (a) Bayer with bilinear demosaicing: 50% contrast reduction (MTF50) at 152 cy/mm, (b) 2PFC^{TM} with bilinear demosaicing: MTF50 at 167 cy/mm, (c) Bayer with state-of-the-art demosaicing: MTF50 at 258 cy/mm, and (d) 2PFC^{TM} with our frequency-based demosaicing: MTF50 at 254 cy/mm. All used 1.40μm pixel pitch. The *ISET RGB* spectra was used for Bayer and the *2PFC-A* spectra was used for 2PFC^{TM}.

FIG. 11: ISET simulations of the J1 region of the ISO12233 chart, with resolution analyzed by "HYRes" according to the CIPA standard and indicated by the red lines. (a) Bayer, Bilinear, 135 l/ph, (b) Bayer, Menon et al.[32], 176 l/ph, (c) 2PFC^{TM}, Bilinear, 174 l/ph, (d) 2PFC^{TM}, spatial demosaic, 177 l/ph, (e) 2PFC^{TM}, Frequency-based demosaic, 177 l/ph. All simulations used 1.55μm pixel pitch. The *ISET RGB* spectra was used for Bayer and the *2PFC-A* spectra was used for 2PFC^{TM}.

FIG. 12: Simulated Macbeth color checker under D65 rendered with ISET at low exposure for (a) Bayer-based sensor with *ISET RGB* filters and (b) 2PFC^{TM} sensor with *2PFC-B* filters.

FIG. 13: (a) Luma and (b) chroma SNR of a simulated 1.4μm-pixels sensor at varying exposure time for two filters sets used with the Bayer CFA (ISET RGB and C-RGB) and two filter sets used with the 2PFC^{TM} CFA (2PFC-A and 2PFC-B).

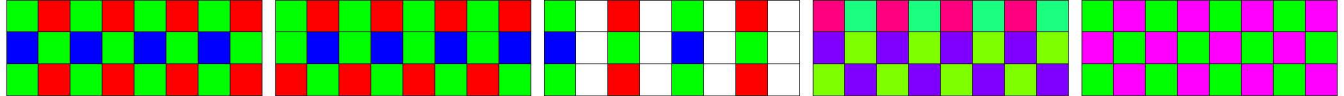

(a) (b) (c) (d) (e)

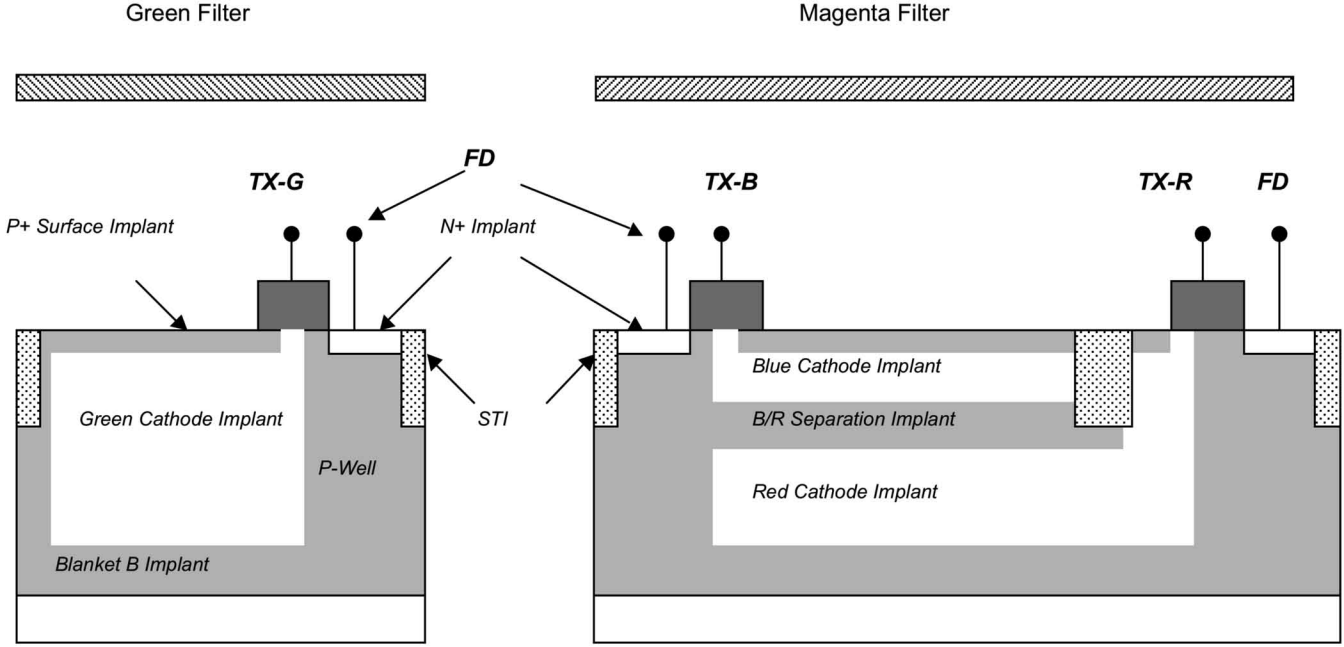
Green Filter
Magenta Filter
FD
TX-G
TX-B
TX-R
FD
P+ Surface Implant
N+ Implant
Green Cathode Implant
STI
P-Well
Blanket B Implant
Blue Cathode Implant
B/R Separation Implant
Red Cathode Implant

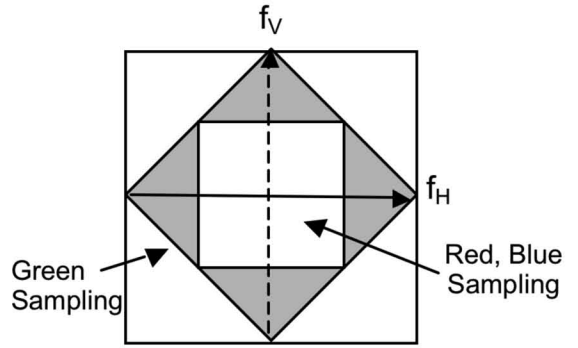
f_V
f_H
Green Sampling
Red, Blue Sampling

(a)

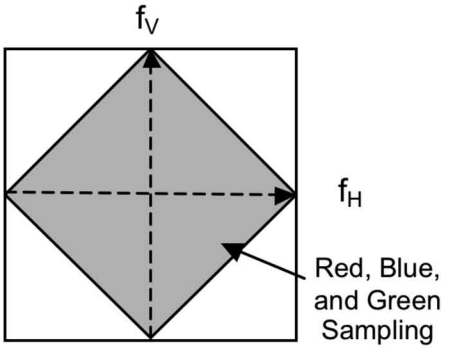
f_V
f_H
Red, Blue, and Green Sampling

(b)

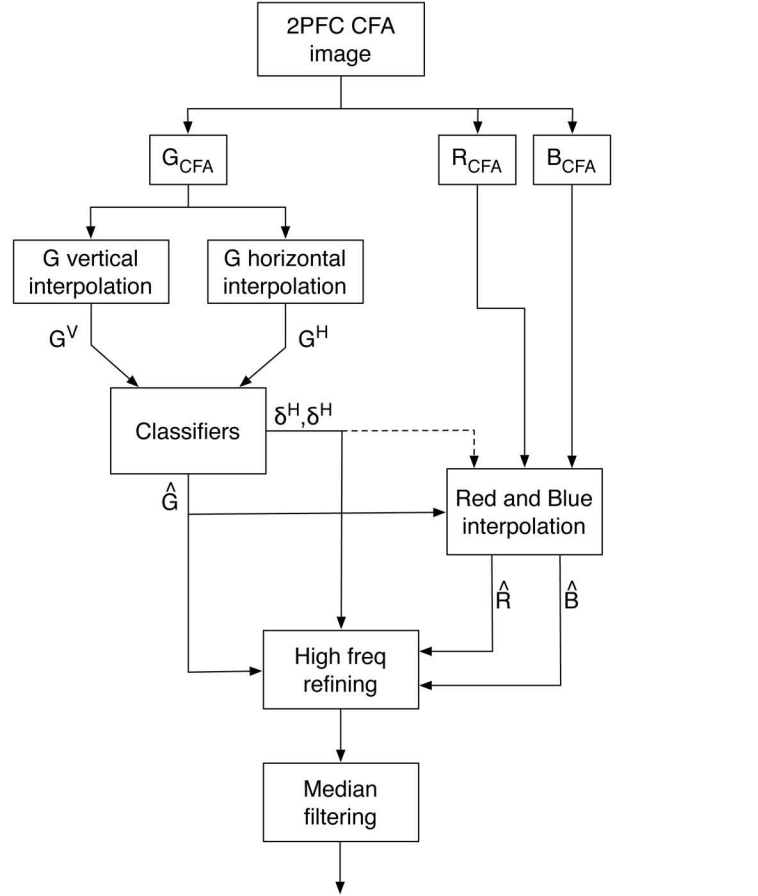
2PFC CFA image
G_{CFA}
R_{CFA}
B_{CFA}
G vertical interpolation
G horizontal interpolation
G^V
G^H
Classifiers
δ^H, δ^H
$\hat{G}$
Red and Blue interpolation
$\hat{R}$
$\hat{B}$
High freq refining
Median filtering

(a)

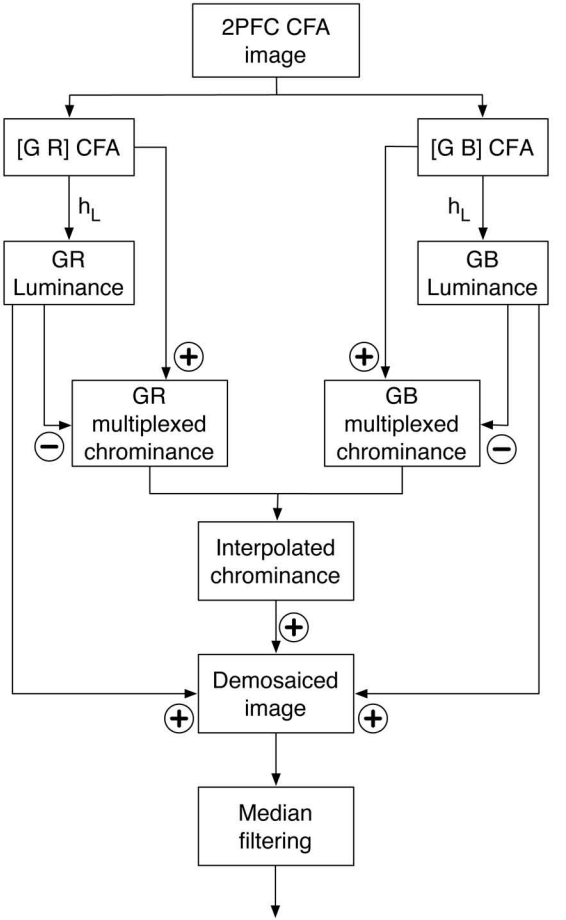
2PFC CFA image
[G R] CFA
[G B] CFA
h_L
h_L
GR Luminance
GB Luminance
GR multiplexed chrominance
GB multiplexed chrominance
Interpolated chrominance
Demosaiced image
Median filtering

(b)

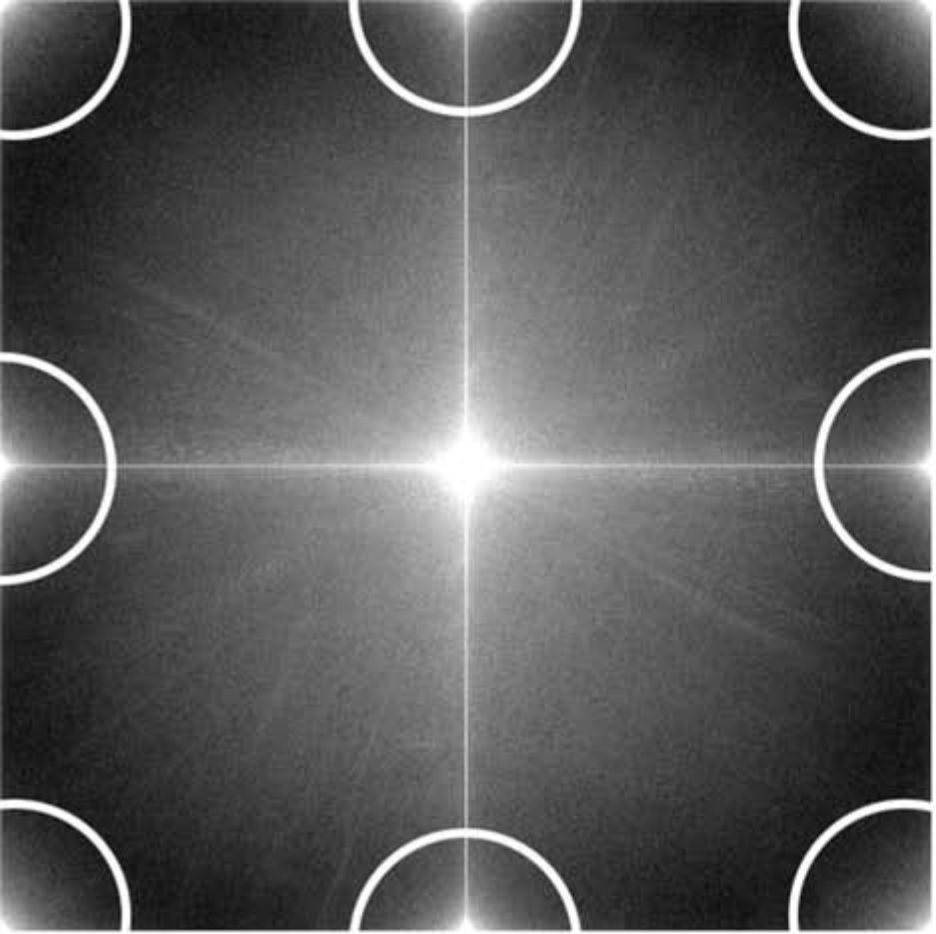

(a)

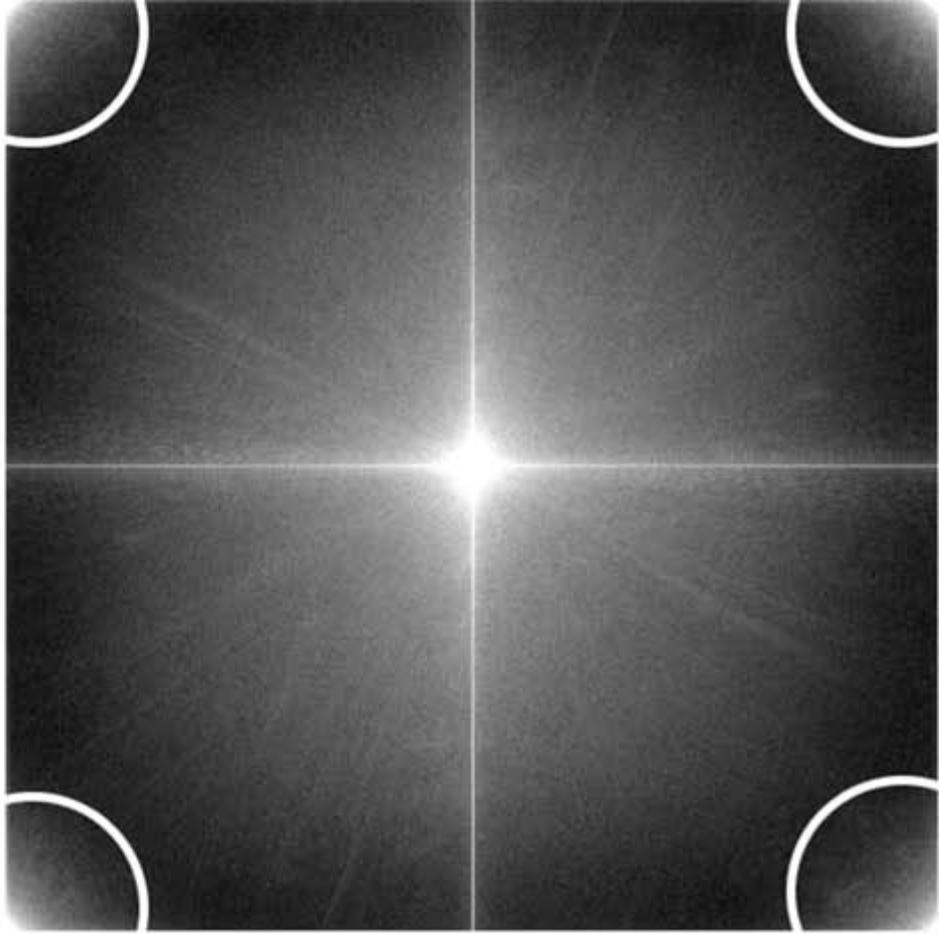

(b)

$$\frac{1}{64}\begin{bmatrix} 0 & 1 & -2 & 1 & 0 \\ 1 & -4 & 6 & -4 & 1 \\ -2 & 6 & 56 & 6 & -2 \\ 1 & -4 & 6 & -4 & 1 \\ 0 & 1 & -2 & 1 & 0 \end{bmatrix}$$

(a)

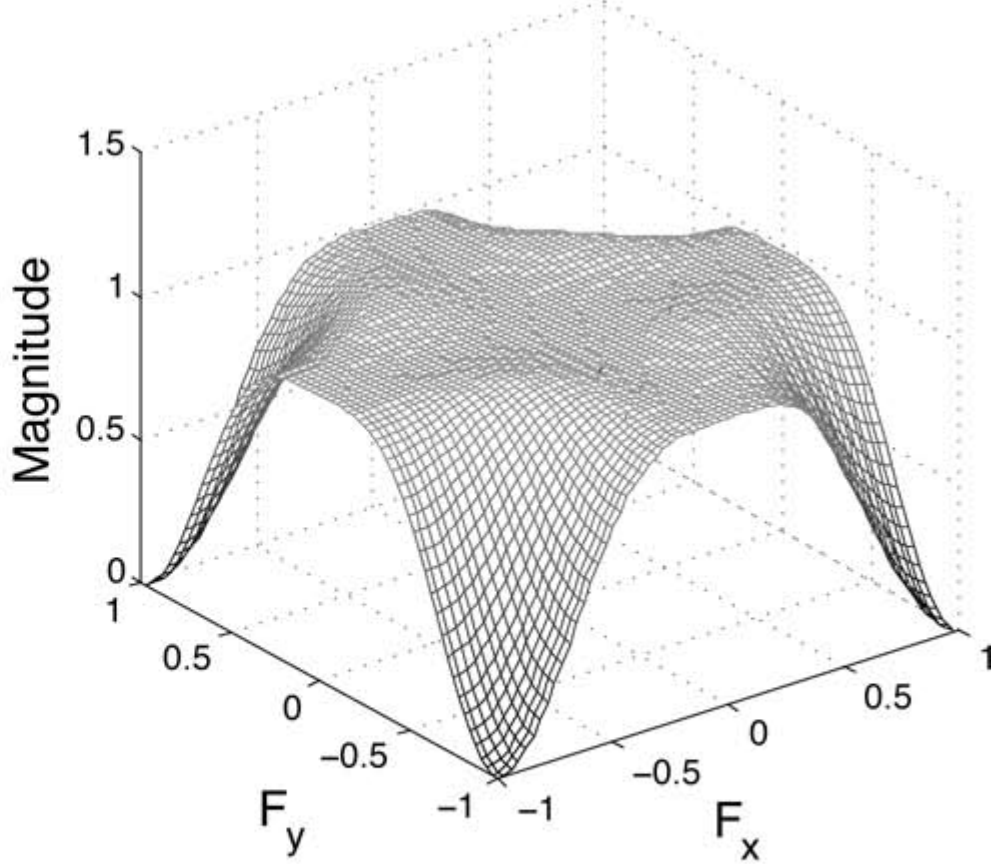

(b)

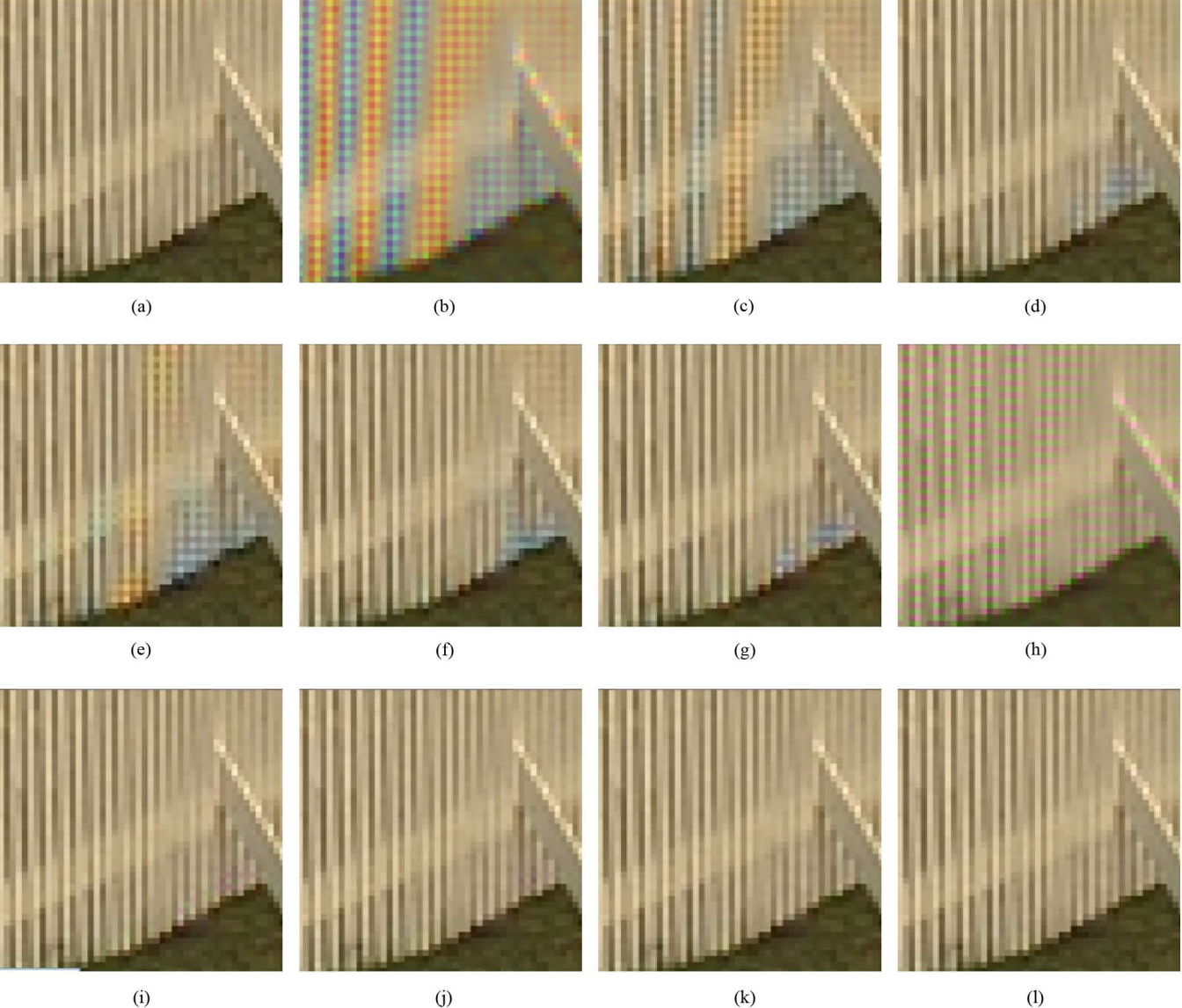

(a) (b) (c) (d)

(e) (f) (g) (h)

(i) (j) (k) (l)

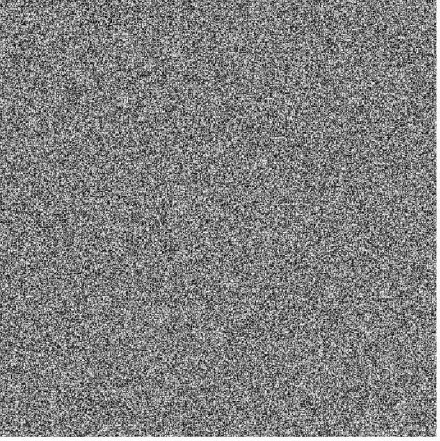

(a)

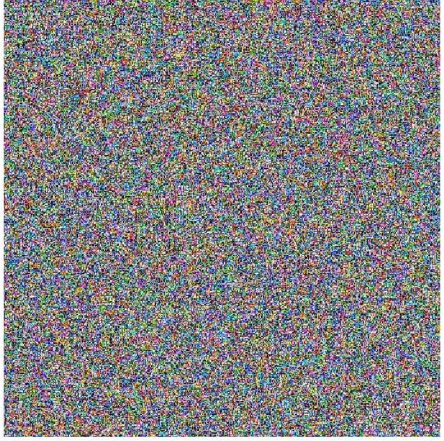

(b)

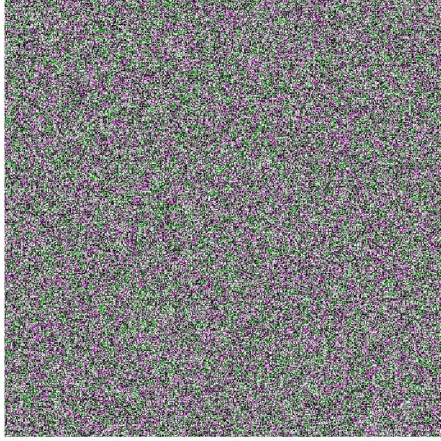

(c)

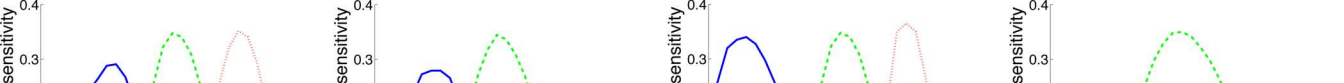
Relative spectral sensitivity
0.4
0.3
0.2
0.1
0
400
450
500
550
600
650
700
Wavelength [nm]

(a) (b) (c) (d)

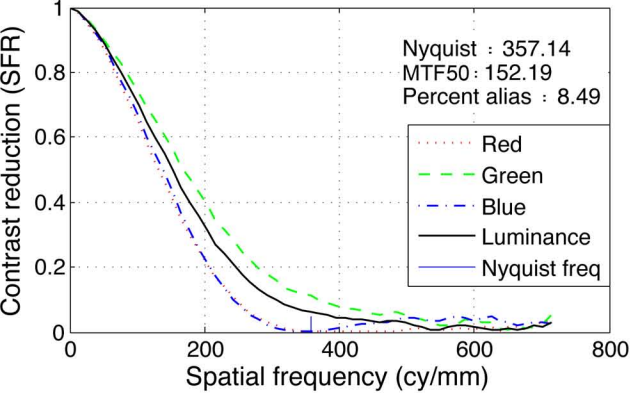
Nyquist : 357.14
MTF50 : 152.19
Percent alias : 8.49
Red
Green
Blue
Luminance
Nyquist freq
Contrast reduction (SFR)
Spatial frequency (cy/mm)

(a)

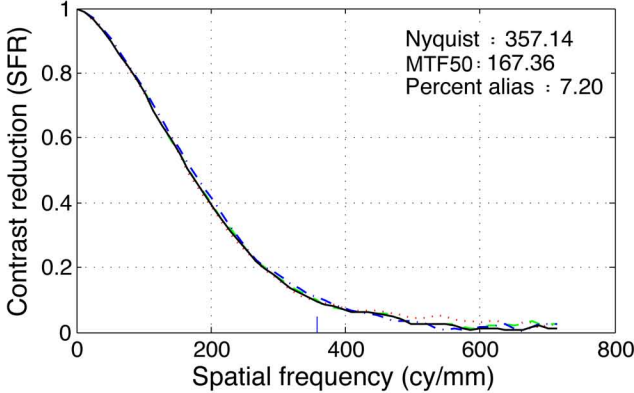
Nyquist : 357.14
MTF50 : 167.36
Percent alias : 7.20
Contrast reduction (SFR)
Spatial frequency (cy/mm)

(b)

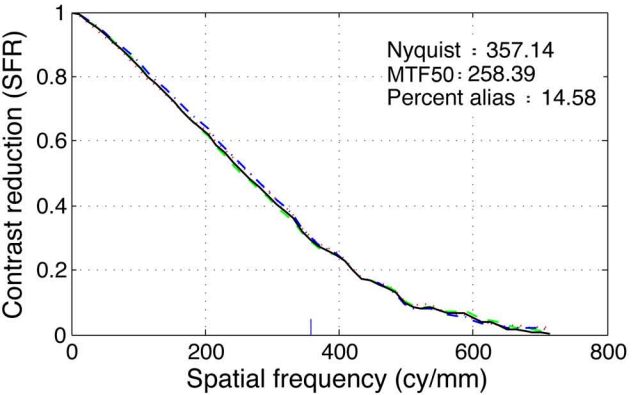
Nyquist : 357.14
MTF50 : 258.39
Percent alias : 14.58
Contrast reduction (SFR)
Spatial frequency (cy/mm)

(c)

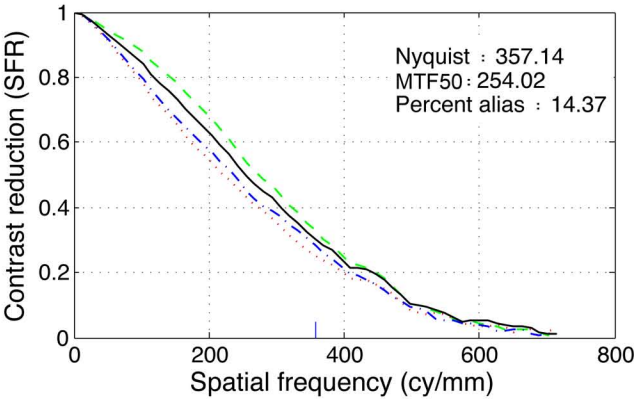
Nyquist : 357.14
MTF50 : 254.02
Percent alias : 14.37
Contrast reduction (SFR)
Spatial frequency (cy/mm)

(d)

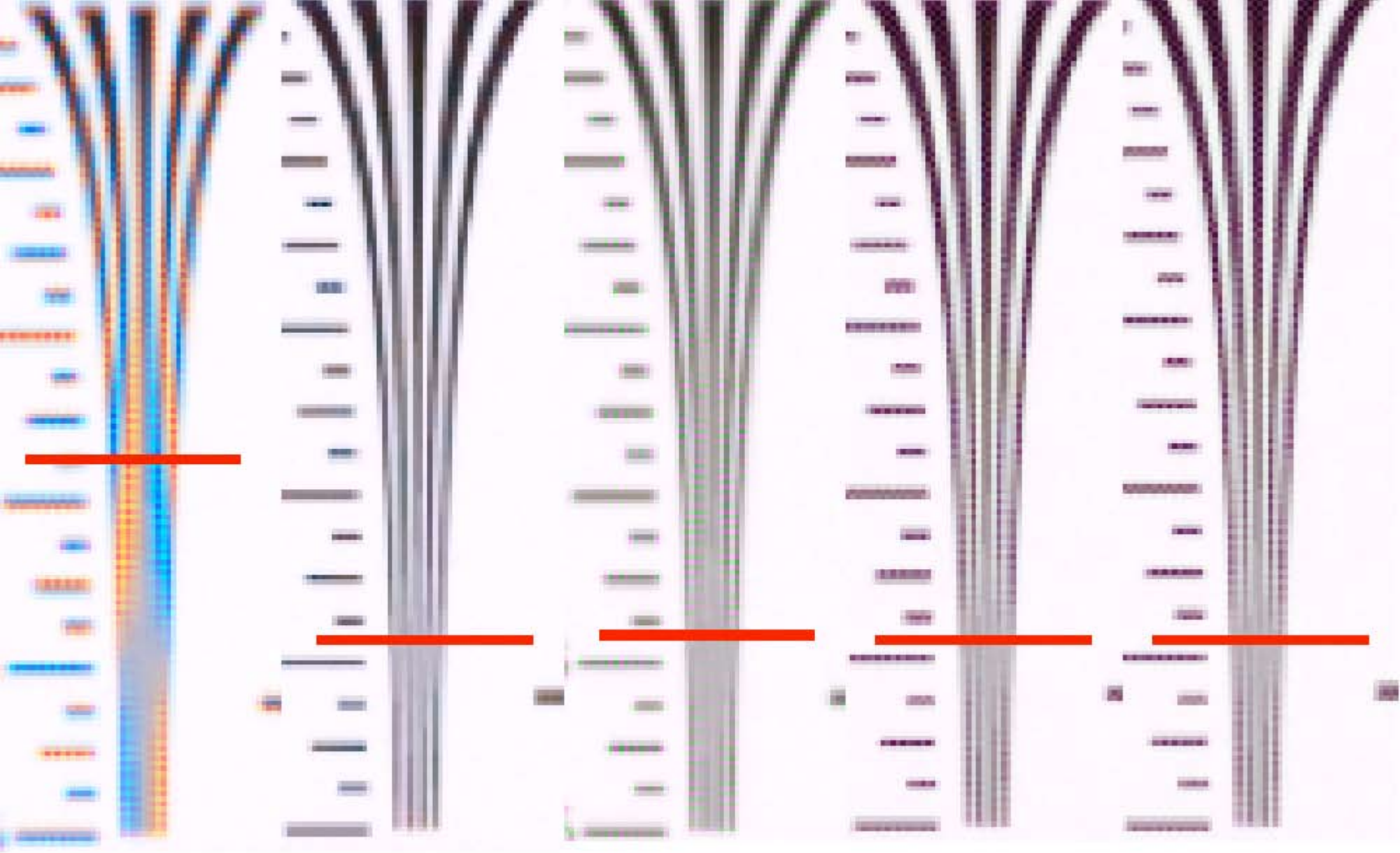
(a)
(b)
(c)
(d)
(e)

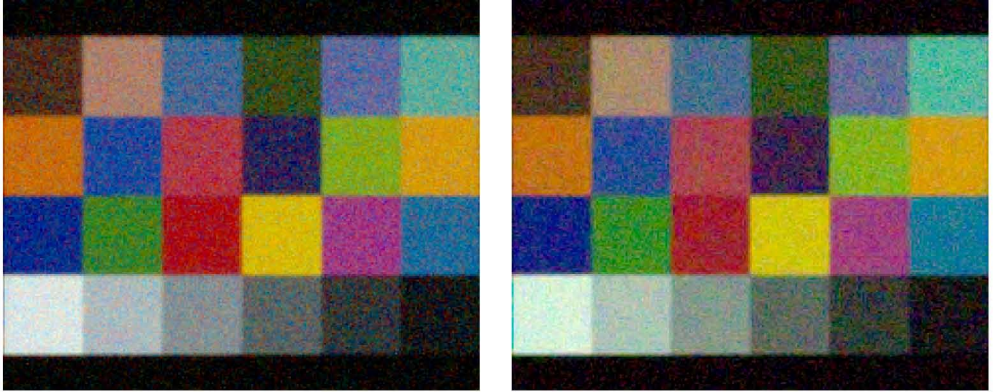

(a) (b)

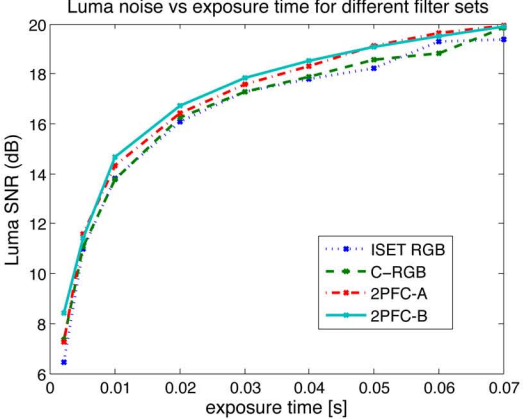
Luma noise vs exposure time for different filter sets
Luma SNR (dB)
exposure time [s]
ISET RGB
C–RGB
2PFC-A
2PFC-B
20
18
16
14
12
10
8
6
0
0.01
0.02
0.03
0.04
0.05
0.06
0.07

(a)

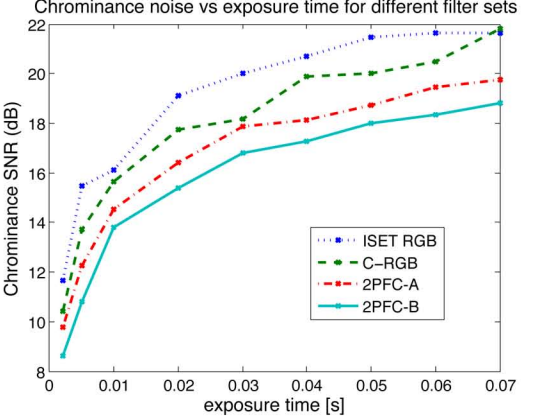
Chrominance noise vs exposure time for different filter sets
Chrominance SNR (dB)
exposure time [s]
ISET RGB
C–RGB
2PFC-A
2PFC-B
22
20
18
16
14
12
10
8
0
0.01
0.02
0.03
0.04
0.05
0.06
0.07

(b)